

# IRAS 18113-2503: the water fountain with the fastest jet?

José F. Gómez<sup>1,2</sup>, J. Ricardo Rizzo<sup>3</sup>, Olga Suárez<sup>4</sup>, Luis F. Miranda<sup>5,6</sup>, Martín A. Guerrero<sup>1</sup>, Gerardo Ramos-Larios<sup>7</sup>

Received \_\_\_\_\_; accepted \_\_\_\_\_

---

<sup>1</sup>Instituto de Astrofísica de Andalucía, CSIC, Apartado 3004, E-18080 Granada, Spain;  
e-mail: jfg@iaa.es

<sup>2</sup>On sabbatical leave at the Australia Telescope National Facility, CSIRO Astronomy & Space Science, Marsfield, NSW 2122, Australia

<sup>3</sup>Centro de Astrobiología, CSIC-INTA, E-28850 Madrid, Spain

<sup>4</sup>UMR 6525 H. Fizeau, Université de Nice Sophia Antipolis, CNRS, OCA. Parc Valrose, 06108 Nice Cedex 2, France

<sup>5</sup>Consejo Superior de Investigaciones Científicas, C/ Serrano 117, E-28006 Madrid, Spain

<sup>6</sup>Departamento de Física Aplicada, Facultade de Ciencias, Universidade de Vigo, E-36310 Vigo, Spain (present address)

<sup>7</sup>Instituto de Astronomía y Meteorología, Av. Vallarta No. 2602, Col. Arcos Vallarta, C.P. 44130 Guadalajara, Jalisco, Mexico

## ABSTRACT

We present Expanded Very Large Array (EVLA) water maser observations at 22 GHz toward the source IRAS 18113–2503. Maser components span over a very high velocity range of  $\simeq 500 \text{ km s}^{-1}$ , the second largest found in a Galactic maser, only surpassed by the high-mass star forming region W49N. Maser components are grouped into a blue and a redshifted cluster, separated by  $0.12''$ . Further mid-IR and radio data suggest that IRAS 18113–2503 is a post-AGB star, thus a new bona fide member of the rare class of “water fountains”. It is the evolved object with the largest total velocity spread in its water masers, and with the highest velocity dispersion within its red- and blue-shifted lobes ( $\simeq 170 \text{ km s}^{-1}$ ). The large total velocity range of emission probably indicates that IRAS 18113-2503 has the fastest jet among the known water fountain stars. On the other hand, the remarkably high velocity dispersion within each lobe may be interpreted in terms of shocks produced by an episode of mass ejection whose velocity increased up to very high values or, alternatively, by projection effects in a jet with a large opening angle and/or precessing motions.

*Subject headings:* masers; stars: AGB and post-AGB; stars: individual (IRAS 18113–2503); stars: mass-loss; stars: winds, outflows

## 1. Introduction

Water fountain (WF) stars are evolved objects with water maser emission spreading over large velocity ranges,  $\gtrsim 100 \text{ km s}^{-1}$  (Likkell & Morris 1988; Imai 2007, for a review). Interferometric observations of water maser components in WFs always show a bipolar distribution, with well defined, spatially separated clusters of blue- and redshifted features (e.g., Imai et al. 2004; Boboltz & Marvel 2005). Moreover, proper motion measurements of these water masers indicate that they trace very collimated jets, with extremely short timescales  $\lesssim 100$  years (see, e.g., Imai et al. 2004). WFs seem to be in the transition between the Asymptotic Giant Branch (AGB) and the planetary nebula (PN) stage, in the phase known as post-AGB, although W43A might still be in the AGB (Imai et al. 2002).

In the late evolution of low- and intermediate-mass stars ( $< 8 - 10 M_{\odot}$ ), the morphology of the detached shells in AGB stars are mostly spherical (Olofsson et al. 2010), while many PNe show clear departures from sphericity, with bipolar or multipolar morphologies. It has been proposed that highly collimated outflows, generated in the late AGB and post-AGB phases could be the main shaping mechanism of PNe (Sahai & Trauger 1998). In this context, WFs could be key objects to understand these shaping processes, since their jets represent one of the first manifestations of collimated mass-loss in evolved low- and intermediate-mass stars.

The number of known WFs is scarce, given the very short timescale of their jets, and that these objects still retain a thick circumstellar envelope, which renders most of them invisible at optical wavelengths. Only 13 candidate WFs have been reported so far, nine of which have been confirmed with interferometric water maser observations (IRAS 16342–3814, Claussen et al. 2009; IRAS 16552–3050, Suárez et al. 2008; IRAS 18286–0959, IRAS 18460–0151, Imai 2007; IRAS 19134+2131, Imai et al. 2004; IRAS 19190+1102, Day et al. 2010; OH 009.1-0.4, Walsh et al. 2009; OH 12.8–0.9, Boboltz & Marvel 2005;

W43A, Imai et al. 2002). We note that interferometric observations of masers are crucial to properly classify a source as a WF. Single-dish observations may not have enough positional accuracy to determine whether the maser emission actually arises from an evolved object or from a nearby source (for instance, a star-forming region), or whether the observed spectrum is the superposition of the emission from several sources.

During a single-dish survey for water maser emission towards optically obscured candidate post-AGB stars and PNe (Gómez et al., in preparation), we discovered a striking spectrum toward the position of IRAS 18113–2503, whose maser components span a velocity range  $\simeq 500 \text{ km s}^{-1}$  that, if confirmed, would be one of the largest found in Galactic masers. Obviously, this source merited further investigation, since it could represent a singular case of extremely high velocity WF.

There is very limited information about this source in the literature. It was cataloged by Preite-Martinez (1988) as a possible PN (object PM 1-221), based on its IRAS data. It was later listed as a candidate proto-PN (Hu et al. 1993; Kohoutek 2001; Szczerba et al. 2007). Its possible nature as a proto-PN (i.e, a post-AGB star) certainly suggests that this could be a new bona fide water fountain.

In this paper, we present new interferometric observations of water masers, carried out with the Expanded Very Large Array (EVLA), to confirm the nature of IRAS 18113–2503 as a water fountain star, and to determine the spatio-kinematical distribution of its maser emission. These observations have allowed us to study the particular properties of this source with extremely high-velocity emission.

## 2. Observations

Observations of the  $6_{16} - 5_{23}$  transition of the water molecule (rest frequency = 22235.08 MHz) were carried with the EVLA (see Perley et al. 2011) of the National Radio Astronomy Observatory<sup>1</sup> in its D configuration on 2010 May 29, towards IRAS 18113–2503 (EVLA project 10A-263). The phase center of the observations was located at R.A.(J2000) =  $18^h14^m27.26^s$ , Dec(J2000) =  $-25^\circ03'00.4''$ , the position of the near infrared counterpart proposed by Ramos-Larios et al. (2009) for IRAS 18113–2503. In order to obtain sufficient velocity coverage and spectral resolution for this source, we set the system to simultaneously observe two overlapping bands in dual polarization, of 320 MHz width each, centered at velocities with respect to the local standard of rest ( $V_{\text{LSR}}$ ) of 40 and 140 km s<sup>−1</sup>, respectively. The resulting combined  $V_{\text{LSR}}$  coverage was from  $-174.8$  to  $356.5$  km s<sup>−1</sup>. Each band was sampled over 256 channels of 125 kHz width (1.7 km s<sup>−1</sup>). We used the source J1331+305 as flux calibrator (assumed flux density = 2.57 Jy, using the VLA 1999.2 coefficients). The source J1820–2528 was the phase calibrator (bootstrapped flux density =  $0.92 \pm 0.05$  Jy), while J1924–2914 was used as bandpass calibrator (bootstrapped flux density =  $13.3 \pm 0.4$  Jy).

All calibration and data reduction was carried out using the Astronomical Image Processing System (AIPS). We followed the current recommendations for reduction of both high-frequency and EVLA data shown in the AIPS cookbook. Data were self-calibrated using the channel with maximum emission in each band, and then applying the phase and amplitude solution to all channels. Maps were obtained with task IMAGR, using a robust weighting scheme of visibilities (with ROBUST = 0) and the CLEAN algorithm for deconvolution. Hanning spectral smoothing was applied to mitigate ringing in the

---

<sup>1</sup>The National Radio Astronomy Observatory is a facility of the National Science Foundation operated under cooperative agreement by Associated Universities, Inc.

bandpass due to the Gibbs effect in the presence of strong, narrow maser lines. The final effective spectral resolution after smoothing is  $\simeq 3.4 \text{ km s}^{-1}$ . The resulting full width at half maximum (FWHM) of the synthesized beam was  $5'' \times 2''$ , P.A. =  $-16^\circ$ , and the noise level in each channel was  $\simeq 0.7 \text{ mJy beam}^{-1}$ . The position of the maser emission in each channel was derived by fitting elliptical Gaussians with task JMFIT.

Following this procedure, we found a significant difference in the nominal position of the emission of the same maser components in the overlapping range of both observed bands. This difference is mainly due to atmospheric phase fluctuations. We used the emission at  $V_{\text{LSR}} \simeq 201 \text{ km s}^{-1}$ , which is present in both bands, to align the whole data set to a common reference position. To make the emission at this velocity coincide in both bands, we shifted the position of all channels in the band centered at  $V_{\text{LSR}} = 40 \text{ km s}^{-1}$  by  $1.13''$ . We consider this as a rough estimate of the absolute positional error in our observations. After the realignment, the relative positional ( $1\sigma$ ) error among different maser components in the map is given by  $\sigma_{\text{pos}} = \theta / (2 \times \text{snr})$ , where  $\theta$  is the FWHM of the synthesized beam, and snr is the signal-to-noise ratio of the maser components. Since most of the maser components found had flux densities  $> 1 \text{ Jy}$ , the relative positional accuracy was typically  $\sigma_{\text{pos}} < 4 \text{ mas}$ .

In order to further study the nature of this source, we have complemented the EVLA data with public archive data from the Wide-field Infrared Survey Explorer (WISE), The Midcourse Space Explorer (MSX), AKARI, and the Infrared Astronomical Satellite (IRAS) space missions.

### 3. Results and discussion

#### 3.1. Spatial distribution and kinematics of water masers

We detected water maser emission in a range from  $V_{\text{LSR}} = -148.7$  to  $350.6 \text{ km s}^{-1}$ . The integrated spectrum in the whole field is shown in Fig. 1a. The position of all maser components is within  $0.15''$  (Fig. 1d), and their spatial distribution is clearly bipolar, clustered in two clumps, with the blueshifted components ( $-148.7$  to  $9.7 \text{ km s}^{-1}$ ) to the north and the redshifted ones ( $177.1$  to  $350.6 \text{ km s}^{-1}$ ) to the south. The intensity-weighted centroids of the blue- and redshifted clusters are separated by  $0.12''$ , with P.A. =  $-14^\circ$ , a separation similar to that found in other water fountain sources (Imai 2007). This clearly suggests that all components arise from the same source, whose position and radial velocity should be approximately midway between those of the two maser clusters. This would mean that the powering source of the maser emission should be at R.A.(J2000) =  $18^h 14^m 26.74^s$ , Dec(J2000) =  $-25^\circ 02' 54.8''$  (absolute error  $\simeq 1.2''$ ), with  $V_{\text{LSR}} \simeq 100 \text{ km s}^{-1}$ . This source would be powering a collimated jet, traced by the maser emission, with a jet velocity of at least  $\simeq 250 \text{ km s}^{-1}$  (half the full velocity range). Neither maser cluster shows a well-defined morphology, like the arcs seen in other water fountain sources (e.g., Boboltz & Marvel 2007; Day et al. 2010), suggestive of bow shocks. They do not show an evident velocity pattern either, although we found a weak correlation in the northern clump, where maser components closer to the central source tend to trace higher velocities (the value of the Spearman’s rank correlation coefficient of velocity vs. distance is  $-0.52$ ,  $p = 0.03$ ).

Since all components seem to arise from the same source, we note that the total velocity range of the emission ( $\simeq 500 \text{ km s}^{-1}$ ) is the second largest ever found in a maser source in the Milky Way, short of the  $\simeq 530 \text{ km s}^{-1}$  detected in the high-mass star-forming region W49N (Morris 1976; Walker et al. 1982). IRAS 18113–2503 is the evolved star (see section 3.2) showing the largest velocity range in their maser emission, superseding by

far OH 009.1–0.4 ( $\simeq 400 \text{ km s}^{-1}$ , Walsh et al. 2009). It is possible that there are maser features at even higher velocities. However, our single-dish observations with the Green Bank Telescope, taken on 2010 February (Gómez et al. in preparation), covered a wider range of velocities ( $-237$  to  $557 \text{ km s}^{-1}$ ), but detected maser components in the same velocity range reported in this paper. Therefore, higher velocity components, if present, should be significantly weaker, below the sensitivity of Green Bank.

IRAS 18113–2503 is also remarkable in the large velocity dispersion within each lobe of the maser jet (see Fig. 1b,c), the largest ever found in a water fountain source. There are several possible explanations for this unusually high velocity dispersion. A possibility is that the jet has large opening angle, so that gas moving on trajectories closer to the plane of the sky will have lower relative radial velocities. We note that the angular size of the cluster indicate an apparent opening angle of the jet of  $\simeq 35^\circ$ , which is relatively large compared with jets in other water fountains, although it is an upper limit to the real opening angle. A conical jet with  $35^\circ$  moving at a constant velocity of  $\simeq 300 \text{ km s}^{-1}$  could have dispersions  $> 150 \text{ km s}^{-1}$  due to projection effects only. A further increase in velocity dispersion could be produced if the jet is precessing (or wobbling). Corkscrew-like motions in masers have been observed in other water fountains (Imai 2007).

An alternative explanation is that the large velocity dispersion in the maser emission is an intrinsic characteristic of the jet. This dispersion is reminiscent of the large velocity width found in the optical knots of the proto-PN Hen 3-1475 (Riera et al. 2003),  $400 - 1000 \text{ km s}^{-1}$ . Riera et al. (2003) interpreted the unusual spectral characteristics of these knots as the result of internal shocks along the jet, generated by episodes of mass loss whose velocity increased with time (Raga et al. 1990). In this scenario, faster material will reach the slower one previously ejected, thus producing a shock that can have large velocity dispersions. We speculate that the water masers in IRAS 18113–2503 could be the result of an ejection



event in which the velocity increased up to a very high velocity, leading to the large velocity dispersion observed in each lobe. Moreover, the presence of recurrent ejection events could lead to shocks and eventually, to maser emission in different locations along the jet (not only at the working surface of its head). This could be the case in other water fountain sources (Claussen et al. 2009; Day et al. 2010). Whether recurrent ejections are common in these objects could be elucidated with time-monitoring studies of their maser emission.

### 3.2. The nature of the central star

Water maser emission can be present in both, young and evolved stars (Elitzur 1992). A usual problem in water-maser-emitting objects is to ascertain its true evolutionary stage. In the case of IRAS 18113–2503, the high-velocity maser emission could be compatible with arising from a high-mass young stellar object (YSO). If this is the case, we would expect it to be associated with a molecular cloud. However, CO(J= 2 – 1) observations toward this source (Rizzo et al. in preparation) failed to detect significant emission, with a stringent upper limit to its main beam brightness temperature,  $3\sigma = 30$  mK. Therefore, we can rule out the YSO hypothesis, and consider the non-detection of CO as a strong proof that IRAS 18113–2503 is a true water fountain evolved star.

Infrared data can shed some further light on the nature of the central star. There are three weak near-IR objects close to this source (labeled A to C in Fig. 2). Neither near-IR (Ramos-Larios et al. 2011), nor Johnson R and I images we took on 2010 July 28 with CAFOS at the 2.2 m telescope of the Calar Alto Observatory, show that any of these objects have peculiar colors that could suggest them to be the powering source of the maser emission. However, at longer wavelengths, WISE data between 3.4 and 22  $\mu$ m show a source with red colors, WISEP J181426.70-250255.6, whose position is compatible with the maser emission (Fig. 2), and with a mid-IR source detected by MSX (source MSX6C

G006.5661-03.6398) and AKARI (source AKARI-IRC-V1 J1814267-250256 in the Point Source Catalog, and AKARI-FIS-V1 J1814268-250304 in the Bright Source Catalog).

A mid-IR spectrum of MSX6C G006.5661-03.6398, extracted from the Spitzer Heritage archive is shown in Fig 3, together with all photometric points found in the MSX, AKARI, IRAS, and WISE catalogs. The Spitzer spectrum shows a broad amorphous silicate absorption at  $18\ \mu\text{m}$ , typical of O-rich stars. Moreover, we note that the photometric data have flux density values very close to those in the Spitzer spectrum. Since those infrared data were taken at different epochs, the flux stability of the source indicates that it is not variable, thus suggesting a post-AGB nature for the central star. Therefore, this further confirms that IRAS 18113–2503 is a new bona fide water fountain.

### 3.3. Comparison with other water fountain sources

IRAS 18113–2503 stands out from other water fountains (Imai 2007) as being the one with the largest spread of line-of-sight velocities in their maser emission ( $500\ \text{km s}^{-1}$ ),  $\simeq 100$  and  $200\ \text{km s}^{-1}$  larger than the first and second runner-ups, OH 009.1–0.4 (Walsh et al. 2009) and IRAS 18460–0151 (Deguchi et al. 2007), respectively. Large maser velocities may indicate that they trace a jet oriented almost along the line of sight. This could certainly be the case of OH 009.1–0.4, for which the bipolar morphology detected by Walsh et al. (2009) is not as clear as that seen in other water fountains. However, IRAS 18113–2503 does show a distinctive bipolar pattern, without any overlapping between the red- and blueshifted lobe.

A study of the proper motions of the maser spots would provide conclusive estimates of the spatial velocity of the jet. Proper motions have been measured in other water fountains with Very Long Baseline Interferometry (e.g., Boboltz & Marvel 2007; Imai

2007; Claussen et al. 2009; Day et al. 2010). These observations also allow the precise determination of distances via parallax measurements, and therefore, the full 3D velocity can be directly measured with high accuracy. The fastest water fountain jet reported with this technique is that of IRAS 18460–0151 (Imai 2007), with a velocity of  $\simeq 300 \text{ km s}^{-1}$ . However, we note that this estimate may be affected by large uncertainties, since large proper motions were measured only for one side of the jet. In the case of IRAS 18113–2503, the projection of the jet velocity on the line of sight can be assumed to be at least half of the total velocity span of the maser, i.e.,  $\simeq 250 \text{ km s}^{-1}$ , and we note that the distinct bipolar pattern provides additional evidence for the presence a significant component on the plane of the sky. Thus, IRAS 18113–2503 is very likely the fastest known water fountain jet.

Proper motion studies will also be key to study the origin of the remarkably high internal velocity dispersion within each lobe, for instance, whether it can be explained with projection effects alone.

JFG and OS acknowledge partial support from Ministerio de Ciencia e Innovación (MICINN) of Spain, grant AYA2008-06189-C03-01. OS, LFM, MAG, and GR-L are partially funded by MICINN grant AYA2008-01934. JRR acknowledges support by MICINN grants AYA2009-07304 and CSD2009-00038. JFG, LFM, and MAG are also supported from Junta de Andalucía (TIC-126). GR-L acknowledges support from CONACyT and PROMEP (Mexico). This research is partly based on observations made with the Spitzer Space Telescope and the obtained from the NASA/ IPAC Infrared Science Archive, both of which are operated by the Jet Propulsion Laboratory, California Institute of Technology under a contract with NASA, on observations with AKARI, a JAXA project with the participation of ESA, and on data products from the Wide-field Infrared Survey Explorer, a joint project of the University of California, Los Angeles, and the Jet Propulsion Laboratory/California Institute of Technology, funded by NASA.

*Facilities:* EVLA, Akari, CAO:2.2m, IRAS, MSX, Spitzer

## REFERENCES

- Boboltz, D. A., & Marvel, K. B. 2005, *ApJ*, 627, L45
- Boboltz, D. A., & Marvel, K. B. 2007, *ApJ*, 665, 680
- Claussen, M. J., Sahai, R., & Morris, M. R. 2009, *ApJ*, 691, 219
- Day, F. M., Pihlström, Y. M., Claussen, M. J., & Sahai, R. 2010, *ApJ*, 713, 986
- Deguchi, S., Nakashima, J.-i., Kwok, S., & Koning, N. 2007, *ApJ*, 664, 1130
- Elitzur, M. 1992, *ARA&A*, 30, 75
- Hu, J. Y., Slijkhuis, S., de Jong, T., & Jiang, B. W. 1993, *A&AS*, 100, 413
- Imai, H., Obara, K., Diamond, P. J., Omodaka, T., & Sasao, T. 2002, *Nature*, 417, 829
- Imai, H., Morris, M., Sahai, R., Hachisuka, K., & Azzollini F., J. R. 2004, *A&A*, 420, 265
- Imai, H. 2007, in *IAU Symp. 242, Astrophysical Masers and Their Environments*, ed. W. Baan & J. Chapman (Cambridge: Cambridge Univ. Press), 279
- Kohoutek, L. 2001, *A&A*, 378, 843
- Likkel, L., & Morris, M. 1988, *ApJ*, 329, 914
- Morris, M. 1976, *ApJ*, 210, 100
- Olofsson, H., Maercker, M., Eriksson, K., Gustafsson, B., & Schöier, F. 2010, *A&A*, 515, A27
- Perley, R. A., Chandler, C. J., Butler, B. J., Wrobel, J. M. 2011, *ApJ Letters*, in press
- Preite-Martinez, A. 1988, *A&AS*, 76, 317

- Raga, A. C., Binette, L., Cantó, J., & Calvet, N. 1990, *ApJ*, 364, 601
- Ramos-Larios, G., Guerrero, M. A., Suárez, O., Miranda, L. F., & Gómez, J. F. 2009, *A&A*, 501, 1207
- Ramos-Larios, G., Guerrero, M. A., Suárez, O., Miranda, L. F., & Gómez, J. F. 2011, *A&A*, submitted
- Riera, A., García-Lario, P., Manchado, A., Bobrowsky, M., & Estalella, R. 2003, *A&A*, 401, 1039
- Sahai, R., & Trauger, J. T. 1998, *AJ*, 116, 1357
- Szczerba, R., Siódmiak, N., Stasińska, G., & Borkowski, J. 2007, *A&A*, 469, 799
- Walker, R. C., Matsakis, D. N., & Garcia-Barreto, J. A. 1982, *ApJ*, 255, 128
- Suárez, O., Gómez, J. F., & Miranda, L. F. 2008, *ApJ*, 689, 430
- Walsh, A. J., Breen, S. L., Bains, I., & Vlemmings, W. H. T. 2009, *MNRAS*, 394, L70

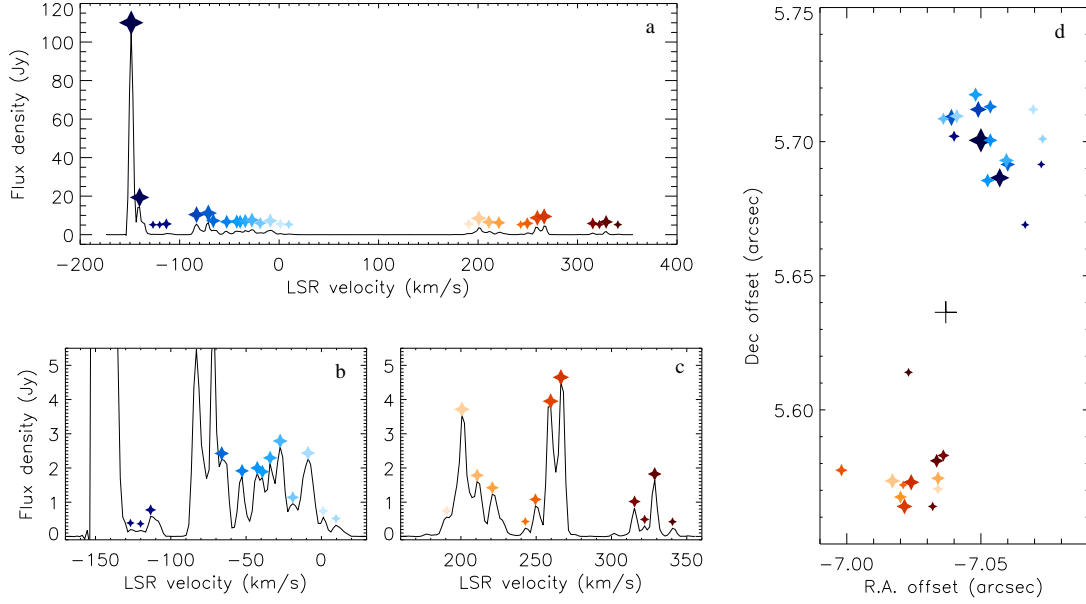


Fig. 1.— (a) Spectrum of the water maser towards IRAS 18113–2503, integrated over an area of  $218.5 \text{ arcsec}^2$ . Colored stars are used to identify each feature in the rest of the panels. (b) Close-up of the blueshifted components. (c) Close-up of the redshifted components. (d) Map of water maser features  $> 0.1 \text{ mJy}$  in IRAS 18113–2503. Axes represent spacial offsets with respect to the phase center of the observations ( $\text{R.A. (J2000)} = 18^h 14^m 27.26^s$ ,  $\text{Dec (J2000)} = -25^\circ 03' 00.4''$ ). The size of the stars is proportional to the logarithm of the flux density of the components. The black cross marks the estimated position of the central source.

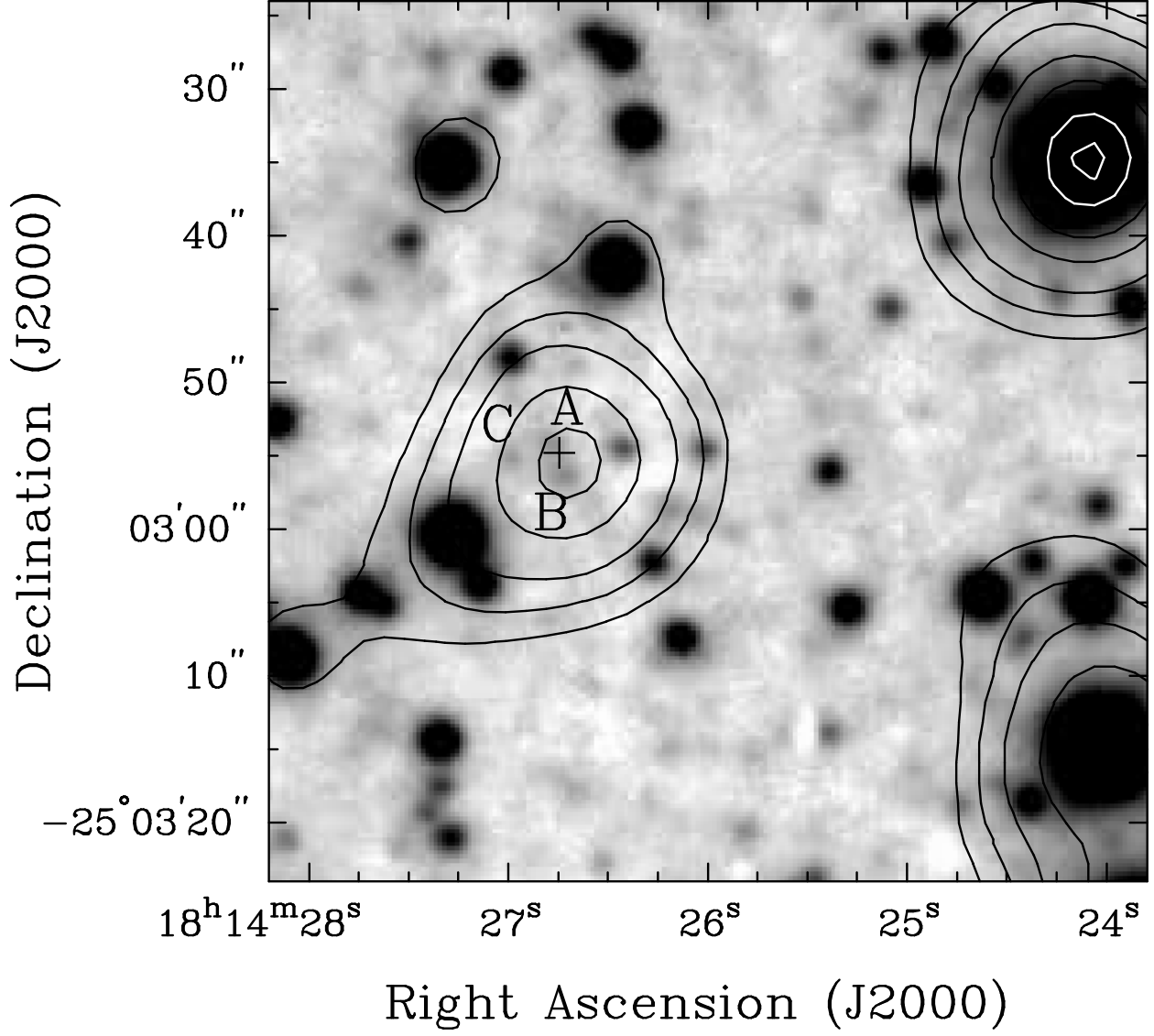


Fig. 2.— Contour map of emission at  $4.6 \mu\text{m}$  from *WISE*, superposed on a near-IR image at  $2.2 \mu\text{m}$  (Ramos-Larios et al. 2011). The cross marks the estimated position of the source pumping the maser emission. The  $2.2 \mu\text{m}$  sources closest to this position are labeled with letters A, B, and C.



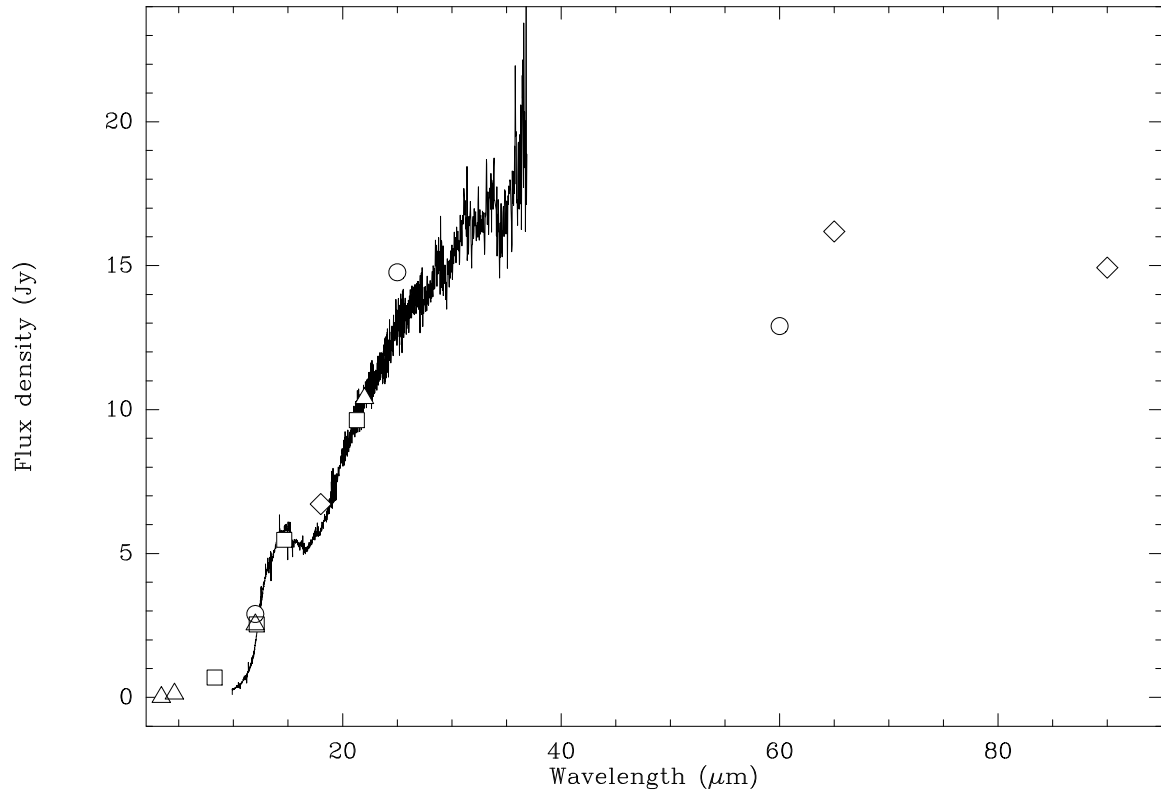


Fig. 3.— Infrared spectra and photometry for IRAS 18113–2503. The solid black line is the Spitzer spectrum. Squares, circles, diamonds, and triangles are MSX, IRAS, AKARI, and WISE data, respectively.